

Co-seismic landslides automatic detection on regional scale with sub-pixel analysis of multi temporal high resolution optical images: Application to southwest of Port au Prince, Haiti

Sumbal Bahar Saba^{1,2}, Muhammad Ali¹, Mark van der Meijde² and Harald van der Werff²

¹ *National Center of Excellence in Geology (NCEG), University of Peshawar, Pakistan,*

² *International Institute for Geo-Information Science and Earth Observation (ITC), Enschede, The Netherlands*

Corresponding author's email: sumbal_saba2000@yahoo.com

Submitted: 20/03/2017, Accepted: 20/10/2017, Published Online: 30/11/2017

Abstract

Customary methods for landslide detection are labor demanding, time consuming and costly. Moreover, it becomes a real challenge to map event triggered landslides using customary techniques. Various automatic and semi-automatic techniques have been proposed for landslide detection. These techniques require extensive technical knowledge and familiarity of the selected study area for visual interpretation, suitable sampling selection, manual parameterization and the trial and error approach for selection of thresholds which makes the process irreproducible. In this context, the purpose of this study is to introduce and investigate the applicability of an automatic technique of Cosi-Corr (Co-registration of Optically Sensed Images and Correlation) for landslide identification on regional scale using high resolution orthorectified worldwies 2 images. Unlike, conventional pixel based semi-automatic methods which depends on spectral properties of pixels, this method is based on pixels shift. The correlation process was performed by using the Cosi-Corr software. The ground displacement field measured from the correlation indicates high displacement values for landslides triggered by 2010 Haiti earthquake. The method automatically identified more than 73% of co-seismic landslides at the threshold value of 3.75. The adopted procedure proposes a quick and economic way for automatic detection of co-seismic landslides on regional scale if suitable pre- and post-event satellite data is available. One limitation of this method is that it does not show any unique behavioral characteristics for different types of landslides so that they could be easily distinguished or classified.

Keywords: Landslides, Landslide detection, COSI-Corr, Haiti.

1. Introduction

Correct and rapid mapping of landslides is essential to know about the full amount and range of landslide disaster (Guzzetti et al., 2004; Tsai et al., 2010) and to create and validate landslide susceptibility models (Guzzetti et al., 2006; Rossi et al., 2010). The ability to effectively detect and monitor landslides and its potential impacts is important to the public, transport authorities, utility companies and the agricultural industry as such phenomena can threaten life, damage infrastructure and have long lasting economic effects.

Customary methods have limitations as data collection techniques are labor demanding, time consuming and costly. Also, accessibility to high mountainous regions is difficult. Moreover, it becomes a real challenge to map event triggered landslides by using customary approaches as happened lately when thousands of landslides were triggered by Kashmir earthquake, 2005, China earthquake, 2008, Haiti earthquake, 2010 and Brazil rainfall, 2011. Therefore, to provide fast and up-to-date landslide information over large areas, various

automatic and semi-automatic landslide detection techniques have been proposed.

The developed methods could be grouped on the basis of type and size of geographical elements used for landslide mapping, such as, pixel-based group (Borghuis et al., 2007; Cheng et al., 2004; Khairunniza-Bejo et al., 2010; Metternicht et al., 2005; Mondini et al., 2011; Yamaguchi et al., 2003) and object-oriented group (Martha et al., 2010; Moine et al., 2009; Park and Chi, 2008; Stumpf and Kerle, 2011). On the basis of number of images used, such as, mono-temporal (Borghuis et al., 2007; Haeberlin et al., 2004) in which single post-event image is used and multi-temporal (Lee and Lee, 2006; Mondini et al., 2011; Nichol and Wong, 2005; Stumpf and Kerle, 2011; Tsai et al., 2010; Weirich and Blesius, 2007) in which two or more pre-and post- event imagery are used.

While using Pixel based approaches, preliminary efforts by Yamaguchi *et al.*, (2003), Cheng et al. (2004) and Lin et al. (2005) focused on semi-automatic landslide detection using low resolution SPOT 1-3 (10-20m) images. Yamaguchi et al. (2003) applied image registration technique using SPOT HRV 10m data and as a result, landslide movement was successfully detected as misregistration vectors between the two satellite images. Likewise, to determine land use changes before and after the landslide occurrence, occurrences, Cheng et al. (2004) used multi-temporal SPOT (20m multispectral) data by performing image classification (image differencing) approach. Similarly, Lin et al. (2005) applied vegetation index differencing method using SPOT data (multispectral 20m). The above cited techniques have benefits and weaknesses. Such as Image registration can be used to measure sub-pixel movement of landslides correctly, but it has great computational cost in terms of CPU time. Similarly, Image-classification reduces the influence of atmospheric, sensor and environmental

alterations among multi-temporal images, but it needs proper selection of adequate training samples to be used for classification. Vegetation index differencing highlights changes in spectral response of various features and decreases influences of topographic effects and illumination. Nevertheless, this method also boosts random noise or coherent noise (Tang and Dai, 2010).

Regardless of the limitations related to these methods, outcomes are vastly reliant on the spatial resolution of the data used for landslide detection. SPOT 1–4 data could hardly be used for detecting and measuring landslides due to its vast spatial extent (Metternicht et al., 2005). Slope failures may be detected using low spatial resolution imagery (SPOT 10m, Landsat TM 30m), only if size and contrast is appropriately large, and very clear. However, according to previous researches, determining landslides types and their causes on spatial scales below 1:25000 are inadequate (Singhroy, 2002). This explains that SPOT (10m) to Landsat TM (30m) imagery have only been utilized to determine landslides related terrain settings, such as, lithology, soil humidity, land use/land cover information and vegetation variation (Cheng et al., 2004; Lin et al., 2002; Mantovani et al., 1996 and Zhou et al., 2002).

After the availability of high resolution (spatial) images (for example, SPOT 5, IKONOS, QuickBird, Cartosat-1 and 2, Worldview1, 2 and ALOS-PRISM data), a new era of research has been initiated for preparing better landslide maps. Research work based on high resolution images include maximum likelihood classifier based change detection comparison by Nichol and Wong, (2005), who proposed the use of medium resolution, multi temporal satellite images (SPOT, XS and IKONOS) for landslide recognition and classification. The results reported up to 70% detection rates. However, the application of this technique require extensive knowledge and familiarity of the

study area for visual interpretation (Khairunniza-Bejo et al., 2010), suitable sampling strategy, and selection of appropriate quantity of training samples to get high detection rate.

A very interesting utilization of high resolution images comes from Hervas et al. (2003) and Rosin and Hervas (2003) who suggested to use computer-generated IKONOS digital imagery at 1-m resolution from existing aerial photographs to detect landslides. In the mentioned method, a new technique for change detection was proposed. The change detection was based on spatial filtering, thresholding and image difference for eliminating pixel clusters related to human induced land use/land cover changes. In the same way, Delacourt et al. (2004) demonstrated semi-automatic approaches to monitor landslide displacement from high resolution multi temporal aerial photographs and Quickbird (0.6m) images. This method has the potential to detect smaller motions on two images acquired with the same sensor. These motions can as low as 0.1 m and gives a very good example that how high resolution images can improve monitoring and mapping of landslides. However, these methods can only be useful to monitor local scale surface changes related to moderate velocity landslides. Major efforts were suggested for applying in a broad range of landslide scenarios in large areas or on regional scale.

All the automatic methods described above are pixel-based methods that depend mainly on the spectral signal of individual pixels. In the last decade, an idea was developed in remote sensing community that pixel-based methods have major limitations in addressing individual landslide characteristic due to finite spatial extent. By applying these methods, geometric and contextual information available in the image are basically ignored (Blaschke, 2010). They suggested a new semi-automatic technique of Object based Image Analysis (OBIA) for

landslides detection based on combination of spectral, morphological, and contextual characteristics of landslides supported by expert knowledge (Barlow et al., 2006; Martha et al., 2010; Moine et al., 2009; Park and Chi, 2008; Parker et al., 2011; Ping et al., 2011; Stumpf and Kerle, 2011).

Primarily, Barlow et al. (2003) used a self-contained classification scheme of OBIA to detect translational landslide scars with overall accuracy of 75 percent. However, landslides below 1 ha in size were ignored in the accuracy assessment. Then, Martin and Franklin (2005) proposed OBIA based approach for detection and separating of soil-lead slides from bedrock-lead slides. For this method, Landsat ETM and DEM data was employed. Approximately 65% classification accuracy was obtained. Barlow et al. (2006) further improved the method by demonstrating an automated classification technique based on image segmentation for discriminating classes of repaid mass movement from SPOT 5 images and a DEM. The overall accuracy was 75 percent, but the detection and classification of individual types have been less successful. To modify the landslide recognition and classification results using OBIA, Martha et al. (2010) developed rules set to synthesize the diagnostic features for semi-automatic detection and classification of landslides using a combination of high resolution image segmentation with DEM data. The overall accuracy was 77 percent. However, the proposed methodology comprises of numerous steps of discrete manual parameterization, and the trial and error nature for selection of thresholds makes the practice irreproducible, cumbersome and lengthy.

The above literature review of pixel based methods illustrates that very few studies have used pixel based approaches for landslide mapping by using high resolution imagery except Delacourta et al. (2004) who

used real high resolution IKONOS imagery instead of simulated images and Borghuis et al. (2007) who employed unsupervised image classification using SPOT-5 imagery for automated landslide mapping (detect 63%). These methods still need to be well explored due to improved spatial resolution imagery (SPOT 5, IKONOS, ALOS, QuickBird and WorldView1-2).

Similarly, the literature review of object based methods reveal that if a semi-automated technique based on OBIA has to be used then the rules set shall be redefined for every area to convert the regions or segments into meaningful objects. For good rules set, good expert based knowledge is required to formulate rules to be incorporated on various stages of the analysis, and introduction of many parameters means introduction of many errors on various stages. Additionally, there are different challenges involved in processing large datasets. OBIA based landslide detection methods also have tendency to miss a mark in conditions where both newly triggered and older landslides are present and therefore it prevents an accurate event-related landslide mapping.

In this context, the purpose of this study is to introduce, explore the applicability and performance of an automatic technique of Cosi-Corr (Co-registration of Optically Sensed Images and Correlation) for landslide identification on regional scale by using multi-temporal high resolution optical images. Unlike, conventional pixel based semi-automatic methods, which depends on spectral properties of pixels, this method is founded on pixels shift. Landslides will be identified on the basis of displacement if during the pre- and post-event period pixels have changed their position. Furthermore, this method is totally automatic, so no rules set with many parameters and thresholds are required to be integrated on different stages of the analysis.

2. Study area

A magnitude Mw 7.0 earthquake hit 15 km southwest of Port-au-Prince region of Haiti on January 12, 2010 at 18°27'25"N latitude and 72°31'59"W longitude. The earthquake happened at a depth of 13 km along the Enriquillo-Plaintain Garden fault zone (EPGFZ). The fault passes west-east laterally to the northern part of the southern Haiti peninsula. It is characterized by evident tectonic geomorphology comprising of long, linear waterway gorges, extensional basins along releasing bends, and north- and south-facing mountain escarpments. Delta fans and alluvial valleys display marks of speedy sedimentation and substantial movement of dynamic drainages over the Quaternary.

Haiti's has generally hot and humid tropical climate. Average temperature ranges from 25°C in January and February to 30°C in July and August. The average annual rainfall is 140 to 200 centimeters. Agricultural practices are common on slope terraces. Deforestation, erosion, land fragmentation and poor primitive agricultural techniques are giving rise to increased land sliding in the area.

In the epicenter zone and in the surrounding valleys, thousands of co-seismic landslides were triggered that caused widespread damage (Eberhard et al., 2010; Ellen et al., 2010). Landslide head scarps and debris avalanche were commonly reported along the sidewalls of the River Momance canyon, within the Mio-Pliocene and older limestone bedrock in steep slopes and road cuts (Koehler and Mann, 2011). Co-seismic landslides and debris fall were evident in river valley with massive debris aprons at the bottom of slopes that every so often refract the river, and masses of rocks and debris were dumped on the river alluvium.

A study site of 120 km² area is selected in the south west of Port-au-Prince (Fig. 1). The

site was selected due to its nearness to the epicenter, its location along the active fault zone (EPGFZ), high concentration of co-seismic landslides and availability of pre-and post-earthquake imagery. The selected area has experienced an intricate geologic past of incursion, tectonics, corrosion, and sedimentation. The topography of the study area is relatively rugged ranges from 0 to 1100m above mean sea level. It has steep mountain ranges and hill-fronts, deeply incised streams with slope ranges from 15° to 60°. The narrow intermountain stream valleys include River Momance and Frorse.

In the study area, the Enriquillo fault system separates basaltic rocks to the south of the fault and sedimentary rocks which consist of sandstone and limestone to the north (Eberhard et al., 2010). The soils in the mountains are thin. The lower hills on west side of the study area have abundance of red clays and loams.

The lithological formations are explained in detail in the following Table. 1, translated from Geologique de la Republique D' Haiti.

Table. 1. Lithological description.

Name (Abbreviation)	Period/System	Lithology
Complex Thoelitique (Cb)	(Cretaceous)	Sedimentary complex of the south island Peninsula (Fm. Demisseau) with massive flows, with or without inter bedded sedimentary and metamorphosed basalt, ultramafic rocks
Pliocene (P)	(Tertiary)	Marls and sands of the central plateau and the big hill Pliocene weakly cemented clastic deposits in fans and low hills
Miocene Inferieur (Mi)	(Tertiary)	Lower Miocene: Sandstone-pelitic flysche Central Plateau calcareous sandstone Basin “Gros Morne” (fm. La Crete) lime stones of the platform chain on Paincroix of the peninsula and South Island
Eocene Moyen a superieur (Ems)	(Tertiary)	Middle to Upper Eocene limestone: (cracked and porous carbonate aquifers high permeable)South Island and southern slopes of the Massif du Nord also have limestone platform of the Massif du Nord
QFP:	Quaternary	Holocene to late Pleistocene fluvial alluvium (channel, terrace, floodplain and over bank deposits)

3. Material and methods

In the following section, the dataset used will be explained briefly accompanied by a short review of the Cosi-Corr technique.

3.1. Satellite Data

The orthorectified worldview-2 data for Haiti provided by Digital Globe as part of digital globe’s crises event services are utilized in this analysis. Pre-event worldview-2 images of 13 Dec 2009 and post-event images dated 15 Jan 2010 were used for the detection of landslides (Table.2). The images were made available in standard format (LV3D) with only RGB bands instead of basic imagery format (Level 1B). Spatial data with level LV3D mean that it had been sensor-corrected, radiometrically-corrected and orthorectified. It was acquired with a mean viewing angle of 15° for pre-event and 16° for post-event imagery.

In order to orthorectify and co-register images upto sub-pixel accuracy level, the availability of data in basic format with the supporting files like RPB and IMD is a prerequisite. However, due to the unavailability of these supporting files, we

used the images in standard format. These images were already orthorectified and radiometrically corrected but from the perception of co-registration, there was a slight shift between the pre- and post-event imagery.

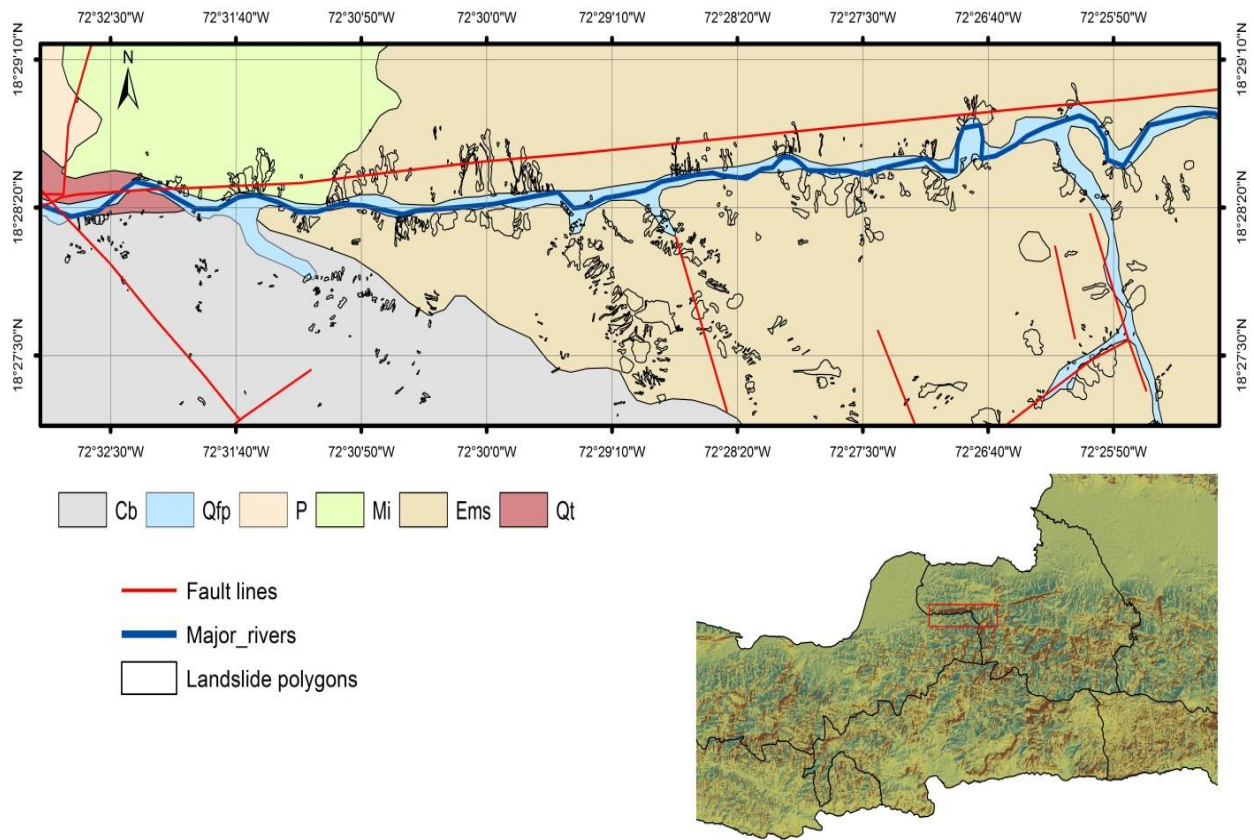


Fig. 1. Shows the location of the selected study area overlapped by earthquake triggered landslides. It is situated in the South of Haiti and adjacent to Portau-Prince. The red color solid lines represent active fault lines passing through the area.

Table 2. Analyzed Worldview-2 images

Image ID WV02	Level of data	Acquisition data (dd-mm-yyyy)	Avg off-nadir angle	Spatial resolution	Time	Band used
09DEC13152914-S3DS_R01C1-052299729020_01_P001.TIF	LV3D	13/12/2009	15°	2m	23:31	Green
10JAN15152539-S3DS_R01C1-052300443020_01_P001.TIF	LV3D	15/1/2010	16°	2m	21:50	Green

Usually 3N band is selected for correlation studies (Ayoub et al., 2008; Scherler et al., 2008; Vermeesch and Drake, 2008). It usually offers the best SNR (signal

to noise ratio) as it has the largest spectral bandwidth. In our case, among the three RGB bands resampled to 2m spatial resolution,

Green band was selected as it has the largest bandwidth after the 3N band (Table. 3).

3.2. Cosi-Corr Technique

A set of techniques/software package/ called Co-Registration of Optically Sensed Images and Correlation (COSI-Corr) described in detail by Leprince et al. (2007) and Scherler et al. (2008) has been used in this study. In this method, precise and accurate image sub pixel level registration and correlation have been attained. The main function of the COSI-Corr is the precise ortho-rectification, co-registration and correlation of the remote sensing data. This software has been developed to detect and measure sub-pixel movement between optical images. In this technique errors due to the imaging system are calibrated and modeled. Topographic artifacts are characterized and solutions are proposed to compensate or to filter them. The technique has been tested and successfully applied in a number of applications by using high and medium resolution data (Avouac et al., 2006; Barisin et al., 2009; Binet and Bollinger, 2005; Dominguez et al., 2003; Herman et al., 2011; Konca et al., 2010; Necsoiu et al., 2009; Scherler et al., 2008). In most of the analyzed cases the co-registration accuracy measured

was in the order of 1/50 to 1/20 of the pixel size (Leprince et al., 2007)

3.3. Correlation

The correlation process was performed by using the Cosi-Corr (Co-registration of Optically Sensed Images and Correlation) software. The pre- and post-event green band with 2m spatial resolution captured at 1° apart off nadir sun angle were used for sub-pixel correlation process. Horizontal displacements were measured by using frequential coorelator method with multi-scale approach where the initial correlation window size was kept at 32 pixels (64m) and final window size as 4 pixels (8m). The step size was set to 2 pixels with 3 iterations. The sub-pixel correlation was calculated in the east-west, and north-south components of the surface horizontal displacement field. In order to correlate the two pre-and post-event images which were not co-registered accurately the output gridded option was deselected. To discard any potential outliers, values with an SNR lower than 0.9, were eliminated. A destripping of the displacement field was executed to suppress attitude residuals produced by undulations of the observing platforms (Leprince et al., 2007; Scherler et al., 2008).

Table 3. Effective band width of WV2.

No	Band name	Effective bandwidth (µm)
1	Coastal	4.730000 x 10 ⁻⁰²
2	Blue	5.430000 x 10 ⁻⁰²
3	Green	6.300000 x 10 ⁻⁰²
4	Yellow	3.740000 x 10 ⁻⁰²
5	Red	5.740000 x 10 ⁻⁰²
6	Red Edge	3.930000 x 10 ⁻⁰²
7	NIR1	9.890000 x 10 ⁻⁰²
8	NIR2	9.960000 x 10 ⁻⁰²

Satellite image data of the selected study site of Haiti encompassed eleven separate image tiles in standard WV2 tiff file format. Supporting data also included a metadata file. The eleven images (Figure 2)

were combined to make a single three band image by the mosaic functionality of ENVI (ITT VIS, 2011).

3.4. Landslide inventory preparation

To better understand the correlation results for the Haiti study area, landslide inventory is prepared by extensive landslide interpretation using high resolution optical satellite images (Worldview-2 and Quick bird) for the pre- and post-earthquake situation. Different landslide types were identified and plotted as polygons by using multi-temporal visual image interpretation. Morphology, vegetation, topography, and drainage conditions of the slopes were the criteria used for landslide identification and classification. Debris flows were combined

as a single landslide type. On locations where two or more than two slides of the same type were sharing boundaries but not scarps were combined as single polygon. Nearly 741 landslides (polygons) with different sizes and types were mapped in the selected study area of 120 km². Out of 741 total landslides, 447 were translational, 294 debris fall and only 4 rotational slides. These landslides are highly concentrated along the south facing slopes of the structurally controlled major rivers of Momance and Frorse.

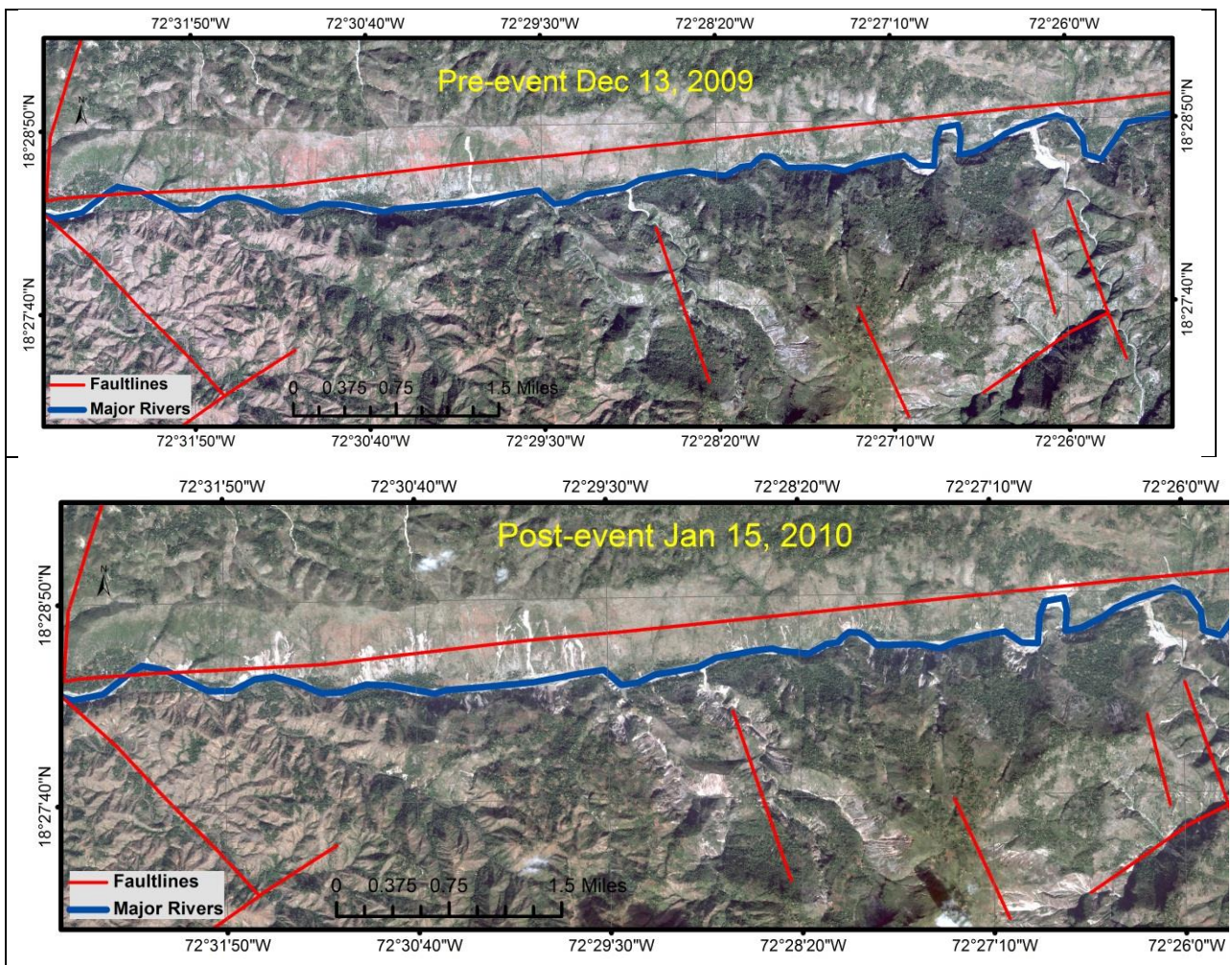


Fig. 2. Shows pre-and post-event worldview-2 images of the study area taken on December 2009 (Pre-Event), and on January 2010 (Post-Event). Red lines outlines major fault system in the area, Blue line represents Momance River

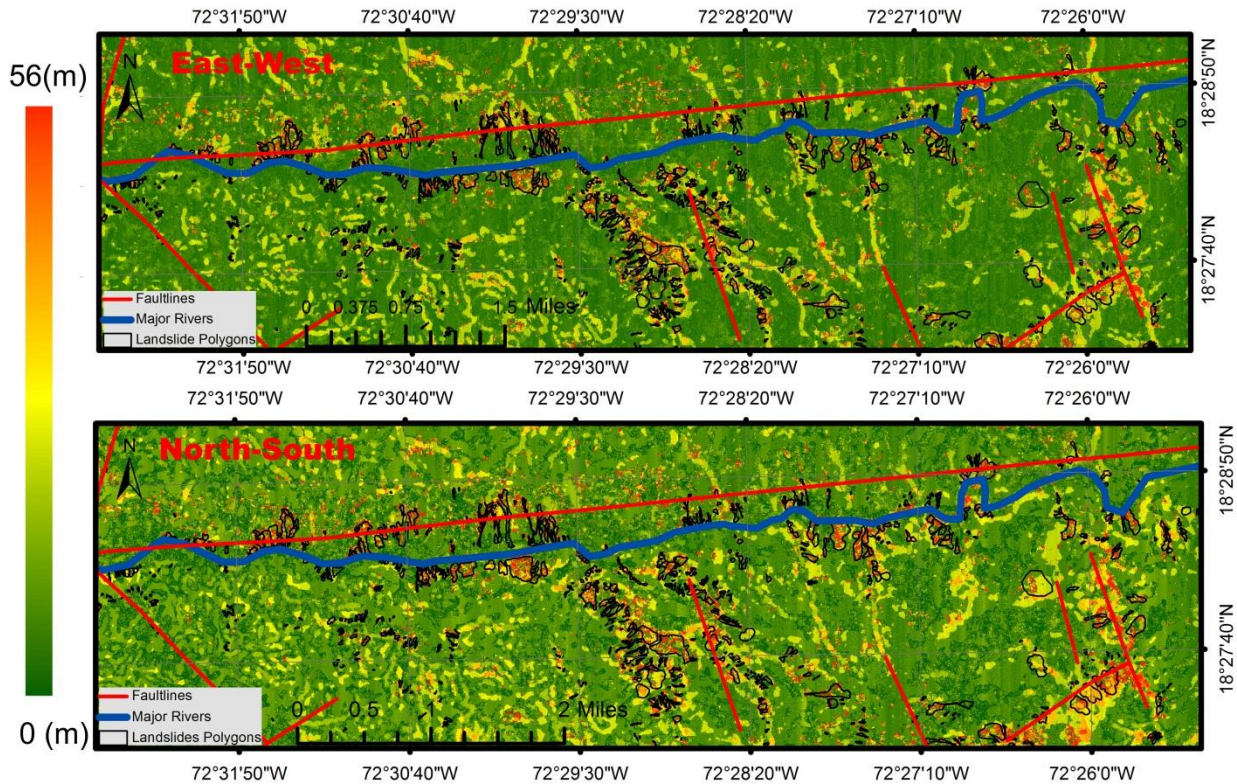


Fig. 3. East-west ground displacement field measured from the cross-correlation worldview-2 images with de-correlated pixels in black. The ground displacement field measured from the correlation of pre- and post-event images reveals high displacement values and decorrelation patches inside the cloud areas. Majority of the area shows no displacement (inside the yellow range of values near to zero displacement).

4. Results and discussion

4.1. Correlation Results

This process produced two correlation images, demonstrating the east–west and north–south horizontal components of the ground displacement field (Fig. 3). The offset is measured in meters. The final spatial resolution of the displacement measurement maps is 6m. The high displacement values that we assume are landslides corresponding very well to the location of the mapped landslides.

Euclidean norm values were calculated by combining the displacement maps for the components of motion in the N-S and E-W directions (Fig.4).

The ground displacement field measured from the correlation indicates high displacement values which agrees very well with the mapped landslide polygons triggered by 2010 Haiti earthquake. However, the high displacement values mostly outspread the landslide boundaries as during the correlation process half of the correlation window is inside the landslide body with totally changed characteristics due to the seismic activity while the other half is outside landslide boundary where things could be recognized but not adequate enough to close the correlation for those parts. The large displacement values mostly coincide with the head or scarp and toe (depositional zones) areas of the landslides with few high displacement values in the center of the landslide bodies (Fig. 4). It also shows high

displacement values for the fault lines and surface breaks.

4.2. Correlation Discussion

We used image pair with only one month time span (32 days, Table.2), therefore, landscape changes due to vegetation and man-made features were limited which reduced the possibility of false positives. Irrespective of the large displacement measurements for the landslide areas except few pixels, there are no de-correlation patches visible in the results even though pre- and post-event images are not totally similar in characteristics. Assessment of the high displacement values (false positives), other than landslides shows that these values have been caused by many lateral surface processes. Which are explained below in more detail.

The pre- and post-event images were not nadir looking but on average captured at 15° and 16° off-nadir sun angle. Although the average off-nadir sun angle was varied by 1° yet it was different for the different tiles of the scenes. The angle of separation between the satellites orbits caused residual topographic artifacts. Visual examination of

the correlation result reveals that due to different sun angles in the scenes to be correlated when, at the scale of the correlation window, shadows orientations have dramatically moved, it caused artifacts (artificial high displacement) in the results.

In literature, it has been suggested that pre- and post-event images should be precisely co-registered as it is reported to be crucial to automated change detection (Lu et al., 2004). In our case, the available data was provided into a pre-processed mode without metadata on processing levels. The relative mis-registration shift between the images was up to 2 meters and varied throughout the study area. Therefore, distortions related to positional shift and parallax artifacts were visible in valley bottoms, concave slopes and rough topographic areas in the form of false positive values (Fig. 3, 4). As the images were given in processed form, therefore, no details were available about the used DEM for the ortho-rectification. Thus, an added source of ambiguity in the correlation maps could also be related with errors in the DEM that can be traced to regions of narrow valleys with high slope and can be azimuth dependent.

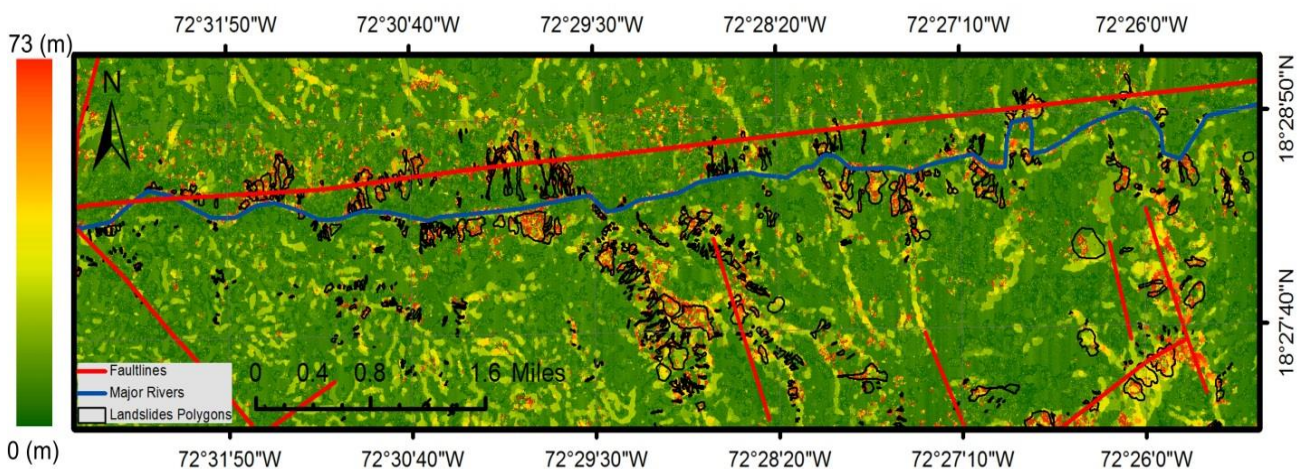


Fig. 4. World-view 2 images correlation results for Haiti earthquake of 2010. The norms of displacement and uncertainties were calculated in the north-south and east-west directions and then added.

In river bed and along the drainage lines the main reason for noise or false positive values was inundation and sedimentation changes by the streams and rivers. This was predominantly visible along the channel of River Momance alluviums. Another reason for large displacement values in the main river bed was the result of sensor saturation, as white sandy areas (also filled with carbonated landslide deposits) appear too bright on the images, and therefore, unrecorded high radiometric difference caused correlation with very high displacement values. In alluviums and deposits areas, measured displacements are > 5 m. Few clouds in the North of the river are also a source of high displacement values in the area.

The results show that vegetation changes or man-made features are not a main concern in this area. The largest displacements are found on landslides and alluviums. On landslide features, observed displacements vary from 3 m to 60 m. Inside the landslide body when the correlation algorithm could not converged the de-correlation noise was then modelled as a zero-mean impulse noise; most of the measurements took arbitrary values within the range allowed by the correlation window size (\pm half the correlation window size). The large displacement values coincide with the scarp and toe of the landslides. Few terrain changes were also noticed due to the seismic activity in the study area as in the correlation map high displacement values are observed along the main fault lines in south east.

4.3. Accuracy assesment results

To assess the quality of correlation results and to find changes related to landslides, correlation result map was classified into “change” and “no-change” classes for 13 threshold values selected at equal population interval of pixels. The results were implemented in the form of

standard error matrices that compares image classification result with ground truth data (Congalton, 1991; Czaplewski and Catts, 1992; van Oort, 2007). Results were plotted in the form of Receiver-Operating Characteristic Curve (ROC) curve which provides a way to select an optimal threshold and to discard sub-optimal ones individually from the class distribution, based on the uncertainty associated with a specific classification threshold. The ROC curve for each classification is determined by calculating the sensitivity and specificity:

$$Sensitivity = \frac{a}{a+b} \quad (1)$$

$$Specificity = \frac{d}{b+d} \quad (2)$$

Where *a* represents true positive, *d* true negatives, *b* false positives, and *c* false negatives

The *sensitivity* of the model is the amount of positive pixels correctly predicted, (*i.e.*, the possibility that a pixel belonging to a certain class is correctly identified). The *specificity* of the model is the fraction of negative pixels correctly predicted (*i.e.*, the probability that a pixel not belonging to a particular category is correctly identified).

4.4. Accuracy assesment discussion/ Comparison with other methods

According to the ROC curve for identification of the changes caused by landslides, the ideal classification threshold shall be 3.75. For which the sensitivity of the model was 0.73, corresponding to a 27% probability of an omission error. In other words on threshold value 3.75 in total 73% of landslides is correctly detected automatically in the selected study area (Table 4).

By selecting a threshold value 3.75 as a cut point between changes and no-changes, we assume that the co-seismic landslides are

the only cause for the changes on the land surfaces. Alterations occurred due to other reasons, including e.g. phenological disparities, agronomic practices and construction, introduce noise which has been addressed in this paper.

One limitation of this method of co-seismic landslides identification is that it does not show any unique behavioral characteristics for different types of landslides so that they could be easily distinguished or classified. This is a limitation, only if the event-inventory is produced for susceptibility, hazard, or risk assessment studies. But, then again in an active circumstance when a disaster struck, fast production of an inventory of co-seismic landslides is more

significant than making of a comprehensive inventory that involves great cost and much time to be consumed. As an alternate, a semi-automatic object based image processing technique could be implemented to detect co-seismic landslides and the sub-types. The OBIA techniques will exploit information extracted from the satellite images and DEMs (Barlow et al., 2006; Martha et al., 2010), but then it will involve extra time and precise expertise to create and tune an appropriate rules set of criteria. Furthermore, object based techniques for landslide detection could not be used for the preparation of event based landslide inventory as OBIA have a tendency to fail when both old and newly triggered landslides are present in the area (Ping et al., 2011).

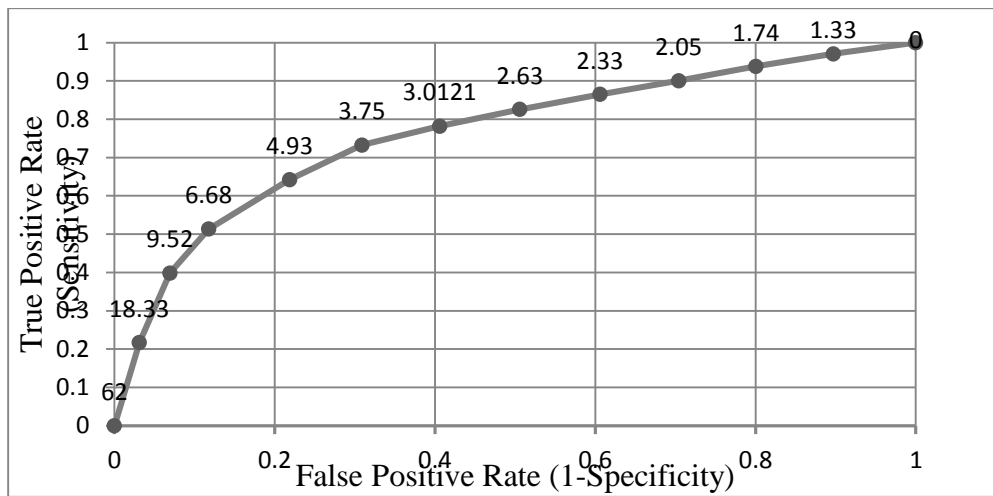


Fig. 5. Receiver-Operating Characteristic Curve (ROC) analysis of the displacement values to observe the shift between true positive and false positive values on each threshold.

Table 4. Accuracy assesment result at threshold value 3.75.

		Classification results					
		slide		No-slide		Total	
Ground Truth data		Area in pixels (1pix=6m*6m)	%	Area in pixels (1pix=6m*6m)	%	Area in pixels (1pix=6m*6m)	%
	slide	66176	73.26%	426985	30.89%	493161	33.48%
	No-slide	24158	26.74%	955509	69.11%	979667	66.52%
	Total	90334	100%	1382494	100%	1472828	100%

4.5. Velocity vectors behavior in different types of landslides

Figure 5 presents the velocity field over the co-seismic landslide areas. High magnitude vectors are more concentrated over landslide bodies, showing high offset values for pixels moved or changed due to landslides. The vectors orientation is arbitrary instead of

downslope trend. The scarp area and depositional zones show high magnitude vectors. Stable areas outside landslide bodies also show some velocity instead of zero displacement most probably due to the fact that various parts of the study area have shifted relatively to each other after the occurrence of the earthquake.

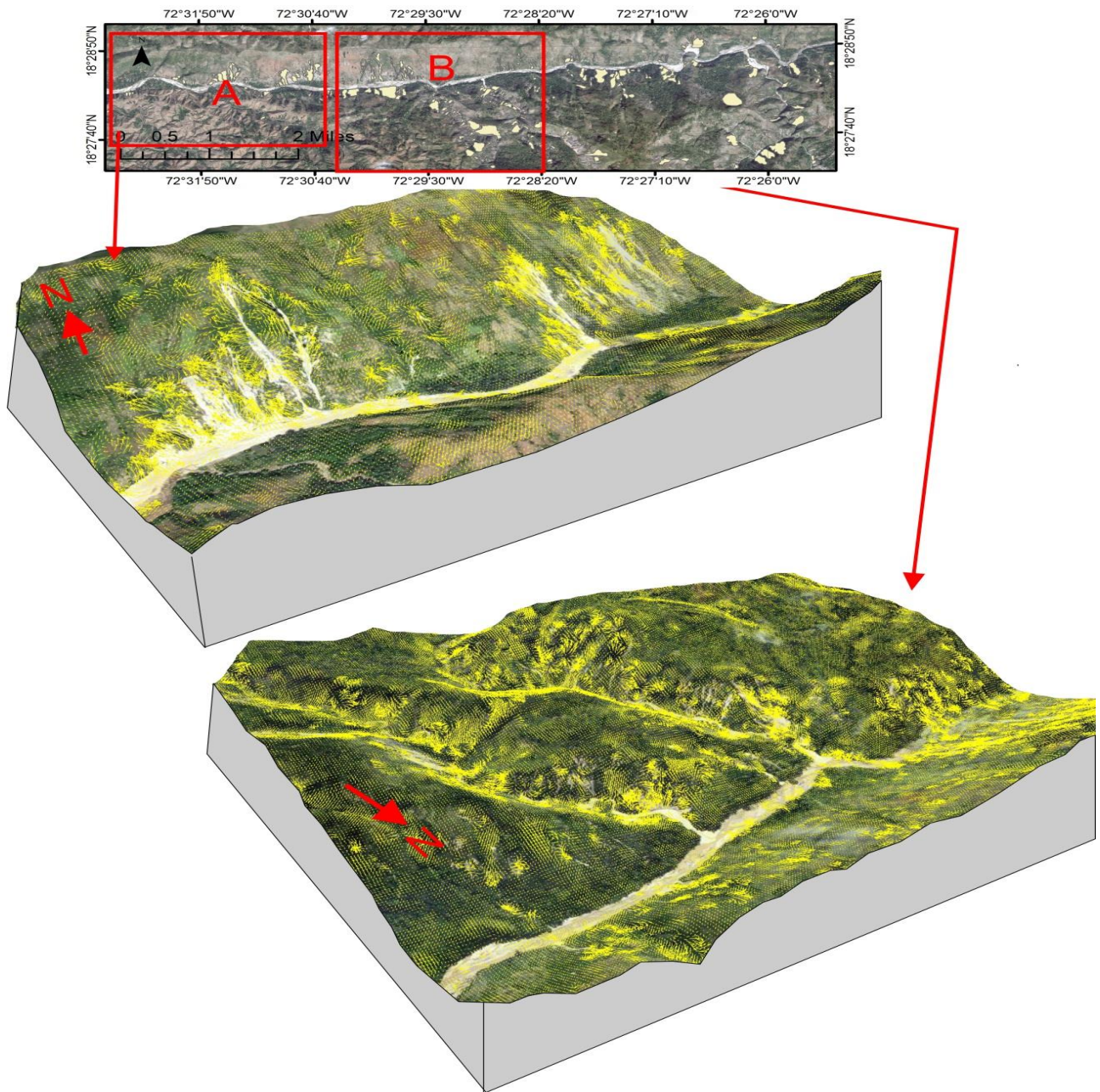


Fig. 6. Vector field plotted from the North/South and East/West displacement maps for two subsections in River Momance valley. It signifies the 2D ground displacement caused by co-seismic landslides.

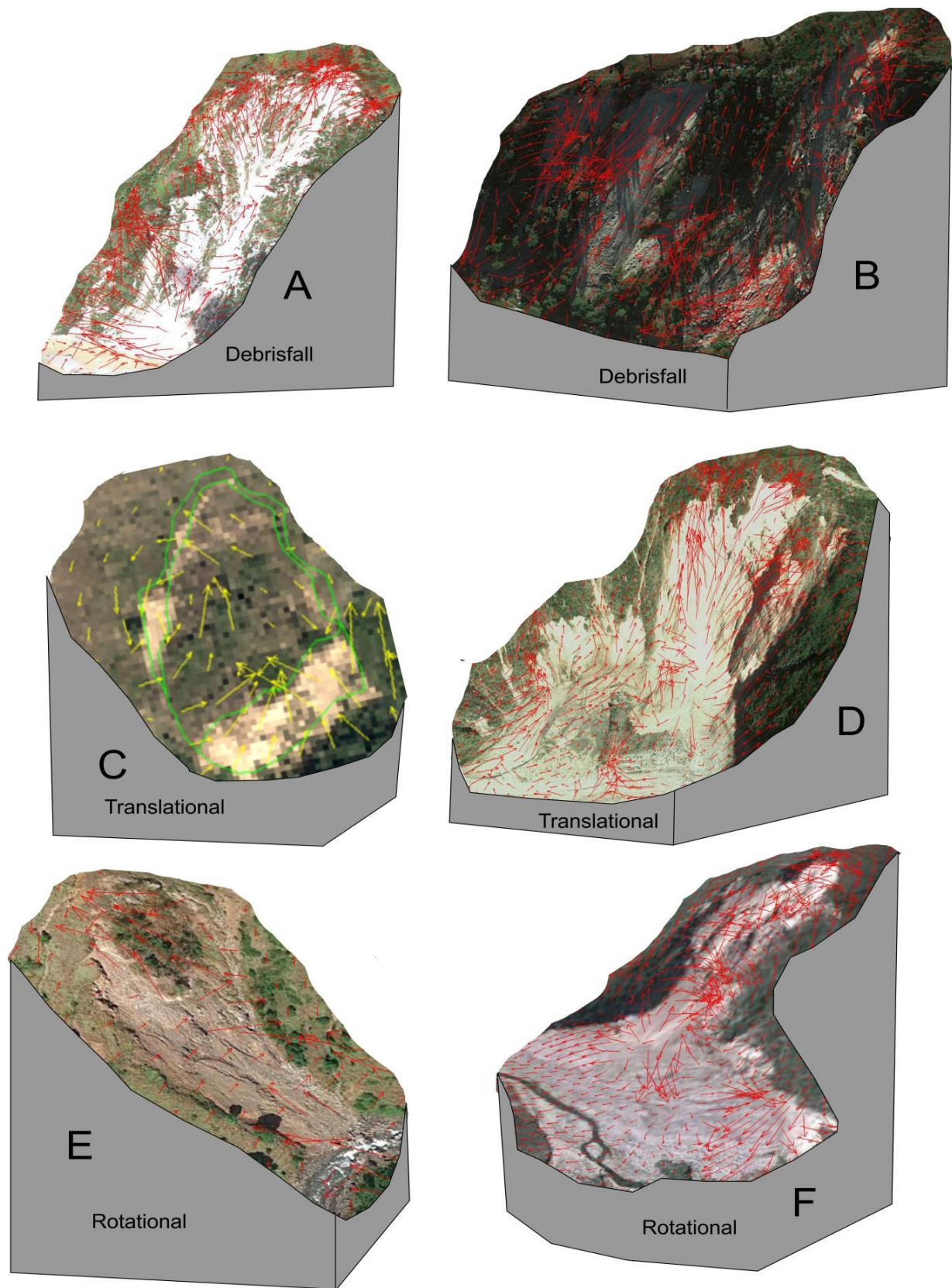


Fig. 7. Magnitude and direction of vectors in different types of landslides

Figure 7 shows velocity field over different types of landslides. Translational and rotational landslides are mainly distinguished on the basis of the geometry of slip surface (Varnes, 1978). Rotational landslides are identified by a curve slip surface and translational landslides are characterized by planar or semi-planar surface. Therefore, translational landslide vectors shall be characterized by equal amplitude vectors from scarp to depositional zone. “A rotational landslide presents for its part a decrease of the ratios of vertical to horizontal displacements, from top to bottom of the landslide”(Casson et al., 2005; Dikau et al., 1996) . In debris fall, there is no specific surface of failure. In the case of translational landslides (Fig.7 C,D) in our study area, it is clearly visible that displacement vectors are not equal on the landslides and neither they are moving downslope. It suggests that landslides do not present a planar slip surface with a translational behavior. These interpretations are the characteristic of a non-uniform landslide behavior. In rotational landslides, the vectors does not seems to take plunge near the head or scarp of the landslide, though it shows concentration of high magnitude vectors. The vectors directions are random and there is no specific pattern visible in different parts of the landslide. Vector directions are arbitrary and mostly indicating upslope movement in all landslide bodies irrespective of the landslide type (translational or rotational). Results also show that even in translational landslides and slumps in which slide bodies were intact and moved few meter, the vector directions were pointing into random directions (Fig. 7C). However, the amplitude of vectors on scarp and depositional areas is high inside all landslide types.

The following few points could be the possible explanation for the random directions of vectors in landslides

- This method has mainly developed to measure horizontal offset within few

(<4m) meters on larger scale instead of measuring larger horizontal offset (>5m) on smaller scale of a landslide.

- Landslides are actually vertical movement on steep slopes from the scarp to the accumulation zones. This method works well for measuring horizontal displacement and it face problems when measuring vertical displacement.
- Due to the total loss of correlation inside landslide body and high velocity for the marginal parts of the landslides, the shift cannot be calculated properly.
- Selecting an added threshold of 0.99 to the signal-to-noise ratio map usually limits the data to low-relief areas and landslides are mostly located on steeper slopes.

5. Conclusions

The paper describes a new automatic technique of COSI-Corr for co-seismic landslide identification on regional scale by using high resolution data. The method successfully identified more than 73% of co-seismic landslides regardless of their size due to the good spatial and temporal resolution of the satellite images. The results show that high magnitude vectors could be used to identify areas of high displacement due to landslides on regional scale but the direction and behavior of vectors could not be used to detect the true direction of slides and distinguish different types of landslides. The adopted procedure proposes a quick and economically way for the preliminary, but reasonably accurate, automatic detection of co-seismic landslides on regional scale if suitable pre- and post-event satellite data is available.

The difference in the sun elevation and slight shift incidence angles of the pre- and post-image adds on in biasing the correlation measurements on topographic

features by showing high false positive values. The results could be further improved by using correctly ortho-rectified and accurately co-registered nadir looking images.

Auhors contrributions

Sumbal Bahar Saba created the data, performed image processing and prepared the manuscript. Muhammad Ali assisted in image processing and provided valuable suggestions to improve the manuscript. Mark van der Meijde and Harald van der Werff contributed to the concept design and improvement of the manuscript.

References

- Avouac, J.-P., Ayoub, F., Leprince, S., Konca, O., Helmberger, D. V., 2006. The 2005, Mw 7.6 Kashmir earthquake: Sub-pixel correlation of ASTER images and seismic waveforms analysis: *Earth and Planetary Science Letters*, 249 (3-4), 514-528.
- Ayoub, F., Leprince, S., Binet, R., Lewis, K. W., Aharonson, O., Avouac, J. P. Influence of camera distortions on satellite image registration and change detection applications, *in Proceedings Geoscience and Remote Sensing Symposium, 2008. IGARSS 2008. IEEE International 7-11 July 2008, 2, p. II-1072-II-1075.*
- Barisin, I., Leprince, S., Parsons, B., Wright, T., 2009. Surface displacements in the September 2005 Afar rifting event from satellite image matching: Asymmetric uplift and faulting: *Geophys. Res. Lett.*, 36 (7), p. L07301.
- Barlow, J., Franklin, S., Martin, Y., 2006. High spatial resolution satellite imagery, DEM derivatives, and image segmentation for the detection of mass wasting processes: *Photogrammetric Engineering & Remote Sensing*, 72 (6), p. 687-692.
- Barlow, J., Martin, Y., Franklin, S. E., 2003. Detecting translational landslide scars using segmentation of Landsat ETM+ and DEM data in the northern Cascade Mountains, British Columbia: *Canadian Journal of Remote Sensing*, 29, 4, p. 510-517.
- Binet, R., Bollinger, L., 2005. Horizontal coseismic deformation of the 2003 Bam (Iran) earthquake measured from SPOT-5 THR satellite imagery: *Geophys. Res. Lett.*, 32 (2) p. L02307.
- Blaschke, T., 2010. Object based image analysis for remote sensing: *ISPRS Journal of Photogrammetry and Remote Sensing*, v. 65 (1) p. 2-16.
- Borghuis, A. M., Chang, K., Lee, H. Y., 2007. Comparison between automated and manual mapping of typhoon-triggered landslides from SPOT-5 imagery: *International Journal of Remote Sensing*, 28 (8), p. 1843-1856.
- Casson, B., Delacourt, C., Allemand, P., 2005. Contribution of multi-temporal remote sensing images to characterize landslide slip surface – Application to the La Clapi`ere landslide (France): *Natural Hazards and Earth System Sciences*, 5, p. 425-437.
- Cheng, K. S., Wei, C., and Chang, S. C., 2004. Locating landslides using multi-temporal satellite images: *Advances in Space Research*, 33 (3) p. 296-301.
- Congalton, R. G., 1991. A review of assessing the accuracy of classifications of remotely sensed data: *Remote Sensing of Environment*, 37 (1), p. 35-46.
- Czaplewski, R. L., Catts, G. P., 1992. Calibration of remotely sensed proportion or area estimates for misclassification error: *Remote Sensing of Environment*, 39 (1), p. 29-43.
- Delacourt, C., Allemand, P., Casson, B., Vadon, H., 2004. Velocity field of the La Clapière landslide measured by the correlation of aerial and QuickBird satellite images: *Geophys. Res. Lett.*, 31 (15), p. L15619.

- Dikau, R., Brunsden, D., Schrott, L., Ibsen, M.-L., 1996. Landslide Recognition. Identification, Movement and Courses, Chichester, etc., Wiley & Sons, 251 p.:
- Dominguez, S., Avouac, J.-P., Michel, R., 2003. Horizontal coseismic deformation of the 1999 Chi-Chi earthquake measured from SPOT satellite images: Implications for the seismic cycle along the western foothills of central Taiwan: *J. Geophys. Res.*, 108 (B2), p. 2083.
- Eberhard, M. O., Baldrige, S. B., Marshall, J., Mooney, W., Rix, G. J., 2010. The MW 7.0 Haiti Earthquake of January 12, 2010: USGS/EERI Advance Reconnaissance Team Report. US Geological Survey Open-File Report, 2010: p.-1048.
- Ellen, R., Jeff, B., Brady, C., Jim, F., Russell, G., Scott, O., Glenn, R., Donald, W., Oscar, S., 2010. Geotechnical Engineering Reconnaissance of the 2010 Haiti Earthquake.
- Guzzetti, F., Cardinali, M., Reichenbach, P., Cipolla, F., Sebastiani, C., Galli, M., Salvati, P., 2004, Landslides triggered by the 23 November 2000 rainfall event in the Imperia Province, Western Liguria, Italy: *Engineering Geology*, 73 (3-4), p. 229-245.
- Guzzetti, F., Reichenbach, P., Ardizzone, F., Cardinali, M., Galli, M., 2006. Estimating the quality of landslide susceptibility models: *Geomorphology*, 81 (1-2), p. 166-184.
- Haeberlin, Y., Turberg, P., Retière, A., Senegas, O., Parriaux, A. Validation of SPOT-5 satellite imagery for Geological Hazard Identification and Risk Assessment for landslides, Mud and Debris Flows in MataGalpa, Nicaragua, *in* Proceedings Proceedings of the XXth ISPRS Congress., Istanbul, Turkey, 2004.
- Herman, F., Anderson, B., Leprince, S., 2011. Mountain glacier velocity variation during a retreat/advance cycle quantified using sub-pixel analysis of ASTER images: *Journal of Glaciology*, 57, p. 197-207.
- Hervás, J., Barredo, J. I., Rosin, P. L., Pasuto, A., Mantovani, F., Silvano, S., 2003. Monitoring landslides from optical remotely sensed imagery: the case history of Tessina landslide, Italy: *Geomorphology*, 54 (1-2), p. 63-75.
- Khairunniza-Bejo, S., Petrou, M., Ganas, A., 2010. Local similarity measure for landslide detection and identification in comparison with the image differencing method: *International Journal of Remote Sensing*, 31 (23), p. 6033-6045.
- Koehler, R. D., Mann, P., 2011. Field observations from the January 12, 2010, Haiti earthquake : implications for seismic hazards and future post-earthquake reconnaissance investigations in Alaska, Fairbanks, Alaska, State of Alaska, Dept. of Natural Resources, Division of Geological & Geophysical Surveys.
- Konca, A. O., Leprince, S., Avouac, J.-P., Helmberger, D. V., 2010. Rupture Process of the 1999 Mw 7.1 Duzce Earthquake from Joint Analysis of SPOT, GPS, InSAR, Strong-Motion, and Teleseismic Data: A Supershear Rupture with Variable Rupture Velocity: *Bulletin of the Seismological Society of America*, 100 (1), p. 267-288.
- Lee, S., Lee, M.-J., 2006. Detecting landslide location using KOMPSAT 1 and its application to landslide-susceptibility mapping at the Gangneung area, Korea: *Advances in Space Research*, 38 (10), p. 2261-2271.
- Leprince, S., Barbot, S., Ayoub, F., Avouac, J. P., 2007. Automatic and Precise Orthorectification, Coregistration, and Subpixel Correlation of Satellite Images, Application to Ground Deformation Measurements: *Geoscience and Remote Sensing*,

- IEEE Transactions on, v. 45 (6), p. 1529-1558.
- Lin, M. L., Wang, K. L., Huang, J. J., 2005. Debris flow run off simulation and verification – case study of Chen-You-Lan Watershed, Taiwan: *Natural Hazards and Earth System Sciences*, 5, p. 439-445.
- Lin, P.-S., Lin, J.-Y., Hung, J.-C., Yang, M.-D., 2002. Assessing debris-flow hazard in a watershed in Taiwan: *Engineering Geology*, 66 (3-4), p. 295-313.
- Mantovani, F., Soeters, R., van Westen, C. J., 1996. Remote sensing techniques for landslide studies and hazard zonation in Europe: *Geomorphology*, 15 (3-4), p. 213-225.
- Martha, T. R., Kerle, N., Jetten, V., van Westen, C. J., Kumar, K. V., 2010. Characterising spectral, spatial and morphometric properties of landslides for semi-automatic detection using object-oriented methods: *Geomorphology*, 116 (1-2), p. 24-36.
- Martin, Y. E., Franklin, S. E., 2005. Classification of soil- and bedrock-dominated landslides in British Columbia using segmentation of satellite imagery and DEM data: *International Journal of Remote Sensing*, 26 (7), p. 1505-1509.
- Metternicht, G., Hurni, L., Gogu, R., 2005. Remote sensing of landslides: An analysis of the potential contribution to geo-spatial systems for hazard assessment in mountainous environments: *Remote Sensing of Environment*, 98 (2-3), p. 284-303.
- Moine, M., Puissant, A., Malet, J., Philippe. Detection of landslides from aerial and satellite images with a semi-automatic method. Application to the Barcelonnette basin (Alpes-de-Haute-Provence, France, *in Proceedings Landslide Processes: from geomorphological mapping to dynamic modellin*, Strasbourg, France 2009, p. 63-68.
- Mondini, A. C., Guzzetti, F., Reichenbach, P., Rossi, M., Cardinali, M., Ardizzone, F., 2011. Semi-automatic recognition and mapping of rainfall induced shallow landslides using optical satellite images: *Remote Sensing of Environment*, 115 (7), p. 1743-1757.
- Necsoiu, M., Leprince, S., Hooper, D. M., Dinwiddie, C. L., McGinnis, R. N., Walter, G. R., 2009. Monitoring migration rates of an active subarctic dune field using optical imagery: *Remote Sensing of Environment*, 113, (11), p. 2441-2447.
- Nichol, J., Wong, M. S., 2005. Satellite remote sensing for detailed landslide inventories using change detection and image fusion: *International Journal of Remote Sensing*, 26 (9), p. 1913 - 1926.
- Park, N. W., Chi, K. H., 2008. Quantitative assessment of landslide susceptibility using high-resolution remote sensing data and a generalized additive model: *International Journal of Remote Sensing*, 29 (1), p. 247-264.
- Parker, R. N., Densmore, A. L., Rosser, N. J., de Michele, M., Li, Y., Huang, R., Whadcoat, S., Petley, D. N., 2011. Mass wasting triggered by the 2008 Wenchuan earthquake is greater than orogenic growth: *Nature Geosci*, 4 (7), p. 449-452.
- Ping, L., Stumpf, A., Kerle, N., Casagli, N., 2011. Object-Oriented Change Detection for Landslide Rapid Mapping: *Geoscience and Remote Sensing Letters, IEEE*, 8 (4), p. 701-705.
- Rossi, M., Guzzetti, F., Reichenbach, P., Mondini, A. C., Peruccacci, S., 2010. Optimal landslide susceptibility zonation based on multiple forecasts: *Geomorphology*, 114, (3), p. 129-142.
- Scherler, D., Leprince, S., Strecker, M. R., 2008. Glacier-surface velocities in

- alpine terrain from optical satellite imagery--Accuracy improvement and quality assessment: *Remote Sensing of Environment*, 112 (10), p. 3806-3819.
- Singhroy, V., 2002. The use of earth Observing Satellites for Hazard Support: Assessment and Scenarios, Final report of the CEOS Disaster Management Support Group.
- Stumpf, A., Kerle, N., 2011. Object-oriented mapping of landslides using Random Forests: *Remote Sensing of Environment*, 115 (10), p. 2564-2577.
- Tang, C.-J., Dai, M. R., 2010. Using Data from an AMI-Associated Sensor Network for Mudslide Areas Identification, *in* Nguyen, N. T., Le, M. T., Świątek, J., eds., *Intelligent Information and Database Systems: Second International Conference, ACIIDS*, Hue City, Vietnam, March 24-26, 2010. Proceedings, Part I: Berlin, Heidelberg, Springer Berlin Heidelberg, p. 380-389.
- Tsai, F., Hwang, J. H., Chen, L. C., Lin, T. H., 2010. Post-disaster assessment of landslides in southern Taiwan after 2009 Typhoon Morakot using remote sensing and spatial analysis: *Nat. Hazards Earth Syst. Sci.*, 10 (10), p. 2179-2190.
- van Oort, P. A. J., 2007. Interpreting the change detection error matrix: *Remote Sensing of Environment*, 108 (1), p. 1-8.
- Varnes, D. J., 1978. Slope movements types and processes, *in* Schuster, R. L., and Krizek, R. L., eds., *Special Report 176 on Landslides: Analysis and Control*: Washington, D.C., Transportation Research Board, National Academy of Sciences, p. 11-33.
- Vermeesch, P., and Drake, N., 2008. Remotely sensed dune celerity and sand flux measurements of the world's fastest barchans (Bodélé, Chad): *Geophys. Res. Lett.*, 35 (24), p. L24404.
- Weirich, F., and Blesius, L., 2007. Comparison of satellite and air photo based landslide susceptibility maps: *Geomorphology*, 87 (4), p. 352-364.
- Yamaguchi, Y., Tanaka, S., Odajima, T., Kamai, T., Tsuchida, S., 2003. Detection of a landslide movement as geometric misregistration in image matching of SPOT HRV data of two different dates: *International Journal of Remote Sensing*, 24 (18), p. 3523 - 3534.
- Zhou, C. H., Lee, C. F., Li, J., Xu, Z. W., 2002. On the spatial relationship between landslides and causative factors on Lantau Island, Hong Kong: *Geomorphology*, 43 (3-4), p. 197-207.